Positron confinement in intermetallic nanoparticles embedded in Fe–Ni–Al material

2004 J. Phys.: Condens. Matter 16 6395

(http://iopscience.iop.org/0953-8984/16/36/006)

INSTITUTE OF PHYSICS PUBLISHING JOURNAL OF PHYSICS: CONDENSED MATTER

J. Phys.: Condens. Matter **16** (2004) 6395–6404 PII: S0953-8984(04)81090-7

Positron confinement in intermetallic nanoparticles embedded in Fe–Ni–Al material

A P Druzhkov[1], **D A Perminov, V L Arbuzov, N N Stepanova and N L Pechorkina**

Institute of Metal Physics, Ural Branch RAS, 18 S Kovalevskaya Street, 620219 Ekaterinburg GSP-170, Russia

E-mail: druzhkov@imp.uran.ru

Received 24 May 2004
Published 27 August 2004
Online at stacks.iop.org/JPhysCM/16/6395
doi:10.1088/0953-8984/16/36/006

Abstract

The affinity-induced positron state was detected in 'defect-free' intermetallic particles using angular correlation of annihilation radiation. It was found that approximately 98% of the positrons annihilate within nanosized and subnanosized intermetallic particles embedded in an fcc Fe–Ni–Al alloy. These particles were created by means of thermal ageing. The ultrafine particles had a structure of the Ni_3Al type with addition of Fe atoms. The nanoparticles were three-dimensional and had no open-volume defects at the interfaces, which could trap a positron. These observations suggest that this positron state promises to be a powerful tool for studies of mesoscopic systems in condensed matter.

1. Introduction

Nanocrystalline particles (nanoparticles) embedded in materials represent an attractive object since they not only show promise for use in quantum devices, but also are of fundamental interest as regards mesoscopic systems. In many cases, atomic structures of nanocrystals are different from bulk structures, because they are strongly affected by environmental host materials. It is therefore very interesting to study electronic and structural properties of such nanoparticles. However, experimental tools for their direct detection have not been available so far since probes employed in conventional methods are not site-selective. Probes equally interact with both nanoparticles and host materials and it is difficult to unambiguously distinguish weak interaction signals from nanoparticles from a much stronger background from the host. The study of nanoparticles requires having a probe that seeks nanoparticles by itself and provides exclusive information about them.

[1] Author to whom any correspondence should be addressed.

It is well known that positrons are sensitive to vacancy-type defects [1]. However, our studies [2, 3] and studies performed recently by other authors [4–6] showed that a positron could be confined in nanoparticles with positron affinities [7, 8] larger than those of the host even if nanoparticles are free from such defects [1]. Authors [4, 5] have called this affinity-induced confinement 'the positron quantum-dot-like state'. A positron in the quantum-dot-like state annihilates only with an electron from nanoparticles and provides site-selective information about their electronic structure in the form of two emitted gamma quanta.

This paper reports detection of positron states in 'defect-free' intermetallic nanoparticles of the Ni_3Al type. Ordered Ni_3Al crystallized to form a cubic structure of the Ll_2 type (γ'-phase) where Al atoms occupied cube corners and Ni atoms were located on cube faces [9]. Nanosized and subnanosized intermetallic particles were formed during thermal ageing of a model fcc Fe–Ni–Al alloy. Ni_3Al precipitates were the most important strengthening phase of Ni-rich alloys (see [10] and references therein). At early stages of ageing ultrafine precipitates of the γ'-phase were homogeneously distributed in the matrix and were fully coherent with the matrix [11].

Positron states in intermetallic nanoparticles were diagnosed by means of angular correlation of annihilation radiation (ACAR), which is a positron annihilation technique [12]. ACAR gives information on electronic properties of the analysed material, specifically the momentum distribution of the valence and core electrons [13]. The core electrons are tightly bound to nuclei and thus high momentum parts of the ACAR spectrum carry information on the type of atom in the region scanned by the positron [14–17]. Therefore the annihilation of trapped positrons with surrounding core electrons reveals chemical information. The study also employs this approach for identifying the local chemical environment of positron annihilation sites.

2. Materials and methods

The Fe–Ni–Al (34.2 wt% Ni, 5.4 wt% Al; C $\leqslant$ 0.01 wt%, the balance Fe) fcc alloy was used. After rolling, cutting and electrical polishing, the samples, about $10\times10\times0.5$ mm^3 in size, were annealed under a 10^{-6} Pa vacuum at 1373 K for 1 h and quenched in water at room temperature. The presence of one austenitic phase in the samples was checked by x-ray analysis. Some of the samples were thermally aged at 823 K for 1–46 h. After each thermal treatment the samples were also quenched in water. It is known [11] that low temperature (823 K) ageing of Ni-rich alloys leads to nucleation and growth of nanosized spherical particles of the ordered ($L1_2$) γ'-phase, which is coherent with the matrix.

The microstructure of the quenched and aged samples was certified using a JEM-200 CX electron microscope at an accelerating voltage of 160 kV (TEM). Samples of the quenched alloys had grains $\sim$50 μm in size and the dislocation densities of about 10^7 cm^{-2}.

To produce vacancy-type defects, some samples of the quenched Fe–Ni–Al alloy were exposed to 5 MeV electrons with a fluence of $\sim0.7\times10^{18}$ cm^{-2} at 300 K in a linear accelerator.

Samples made of well-annealed pure Al, Ni and Fe and monocrystalline Ni_3Al and Ni_3Al–Fe compounds were also used in ACAR measurements as references. The monocrystalline compounds with different chemical compositions ($Ni_{75.3}Al_{24.7}$ and $Ni_{71}Al_{21}Fe_8$) were grown by the Bridgman method (see [18] and references therein).

The ACAR method was realized in a one-dimensional ACAR spectrometer providing a resolution of 1 mrad $\times$ 160 mrad [16]. A ^{68}Ge positron source of activity of 400 MBq was used. At least 8×10^5 coincidence counts were collected in each ACAR spectrum; the peak-to-background ratio was $\sim10^3$. The ACAR spectra represented the dependence of the coincidence count rate on the angle θ (θ being the deviation of the annihilation

γ-quanta from anticollinearity). The angle $\theta = p_z/m_0c$, where p_z is the transverse component of the momentum of an electron–positron pair, m_0 is the rest mass of an electron and c is the light velocity. The ACAR data contain information about the momentum distribution of annihilating electrons [13] and it is possible to separate contributions from annihilation of positrons with nearly free electrons (the low momentum part of the spectrum) and core electrons (the high momentum part of the spectrum). The lattice crystal field has little effect on strongly bound (core) electrons and, therefore, the high momentum part of the ACAR spectrum bears information about the type of atom at a positron annihilation site.

The ACAR spectra of the compounds, the alloys and Ni, Fe and Al, were approximated by an inverted parabola and a Gaussian. The approximation of the experimental spectra considering the spectrometer resolution function has been described in detail elsewhere [19]. The approximation quality criterion approached unity.

The parabolic component may be represented as

$$I_p(\theta) = h_p[1 - (\theta/\theta_p)^2]f(|\theta| - \theta_p), \tag{1}$$

where $f(|\theta| - \theta_p)$ (which is equal to 1 if $|\theta| \leqslant \theta_p$ and 0 if $|\theta| > \theta_p$) is the Heaviside unit function; h_p is the parabola height; and θ_p is the cut-off angle (the angle at which $I_p(\theta)$ values become zero).

According to the free electron approximation for metals, θ_p allows calculation of the number of electrons per atom N_p [20]:

$$N_p = 1.46 \times 10^{-4}(a\theta_p)^3, \tag{2}$$

where a is the lattice parameter in ångströms and θ_p is measured in milliradians. For simple metals, N_p is equal to the number of s-like electrons. For transition metals, N_p is larger than the number of s electrons because of s–d hybridization and corresponds to the number of nearly free electrons (NFEs) [3].

The contribution of core electrons to ACAR spectra was determined from ratio curves [15, 17]. The latter were obtained in the following way: approximated ACAR spectra were normalized to unit area and then Fe–Ni–Al and Ni_3Al spectra were divided by spectra of reference elements. Ni and Al have been taken as the reference elements, since nickel and aluminium are parts of the compound and, in addition, aluminium has a relatively simple structure of the ion core.

Changes of the shape of ACAR spectra were also characterized by standard S- and W-parameters [16]. The S- and W-parameters were defined as the ratios of the sum of the coincidence count rate at θ from 0 to 3.5 mrad and 15 to 25 mrad to the full coincidence count rate, respectively. The S- and W-parameters characterized the probability of annihilation of positrons with NFEs and core electrons respectively. When positrons were trapped in open-volume defects, the S-parameter increased and the W-parameter diminished [21].

3. Results and discussion

Figure 1 shows ratio curves of ACAR spectra for as-quenched Fe–Ni–Al together with those for pure Fe and Ni with respect to the ACAR spectrum of pure Al. These ratio curves directly reflect the contribution of core electrons, because the contribution of intrinsic Al core electrons (mainly 2p states) was small enough [22]. The ratio curves of all the samples represented a peak with a maximum over the interval of momenta (8–11) $\times 10^{-3}$ m_0c, which was due to positron annihilation with 3d electrons of transition metals [15]. As the number of 3d electrons increased (from six in Fe to eight in Ni), the peak got higher and the peak maximum shifted towards larger momentums in accordance with calculation results [22]. The ratio curve of the

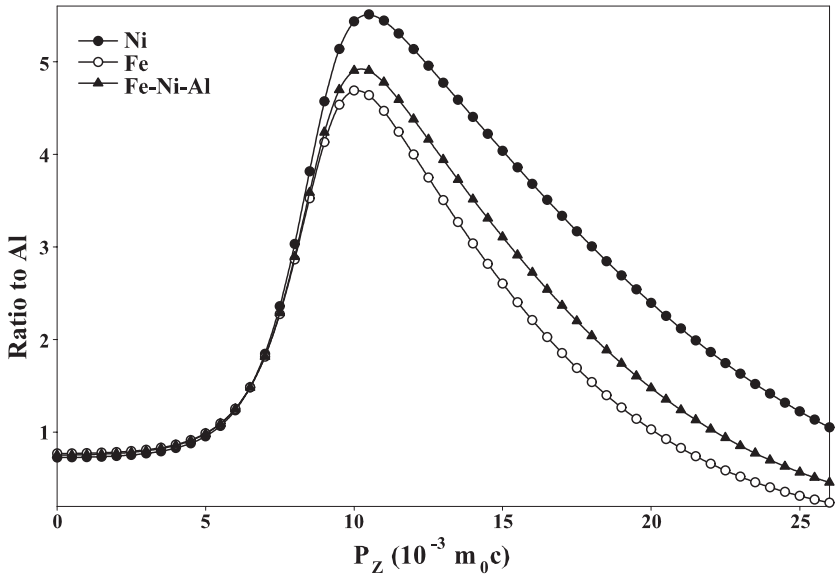

Figure 1. Ratio curves of the ACAR spectra of Ni, Fe and Fe–Ni–Al alloy as quenched, with respect to that of Al.

Fe–Ni–Al alloy was intermediate between the ratio curves of Fe and Ni in accordance with the chemical composition of the alloy. Hence, it may be inferred that positrons did not have significant preferred affinity for either Fe or Ni atoms, while the contribution of Al atoms to the annihilation was small.

Figure 2 presents ratio curves of pure Ni and a Ni_3Al (bulk) single crystal with respect to Al. The ratio curve of the intermetallic is similar to the ratio curve of Ni. This is an indication that positrons annihilated mainly in the Ni sublattice, as was supposed in earlier works [23–26]. In these works it was shown that in Ni_3Al the 'free' positron lifetime τ_f is lower than expected according to a linear interpolation of the τ_f values of the constituent pure metals Ni and Al. This may by due to a charge transfer of $\sim$0.6 electrons from an Al atom to the Ni atoms [27, 28]. This charge transfer gives rise to an enhancement of the positron wavefunction on the transition-metal sublattice and, therefore, to a shift of the τ_f value towards that of pure Ni. Thus, both the ACAR data and the lifetime measurements showed that positrons annihilated predominantly in the Ni sublattice of Ni_3Al.

The peak for Ni_3Al (see figure 2) could diminish for three reasons:

(1) some positrons were trapped in defects such as structural vacancies and then annihilated mainly with low momentum NFEs;
(2) some 3d electrons of Ni atoms and 3p electrons of Al atoms were localized to form strong covalent bonds due to strong Ni d–Al p hybridization between nearest-neighbour Ni–Al atom pairs [28]; as a result, the probability of positron annihilation with 3d electrons of Ni atoms decreased;
(3) the effect of the Ni atom density in the compound.

As far as the first reason is concerned, as mentioned above, the lifetime of positrons in Ni_3Al (bulk) approached their lifetime in well-annealed pure Ni. This lifetime characterized the 'free' delocalized state of positrons in the crystal lattice (see table 1 in [24]) and demonstrated the absence of quenched-in thermal or structural vacancies (the detection limit of the atomic

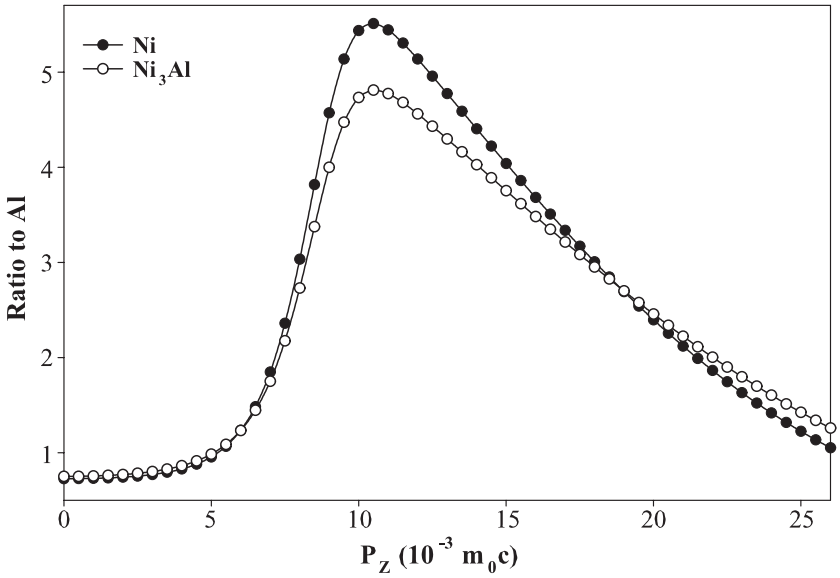

Figure 2. Ratio curves of the ACAR spectra of Ni and Ni_3Al (bulk) with respect to that of Al.

Table 1. Parameters of the ACAR spectra of several materials.

Samples	Site of positron annihilation	*S*-parameter (arb. units)	*W*-parameter (arb. units)	θ_p (mrad) ± 0.01	N_p (electron per atom)
Ni	Matrix	0.518 ± 0.001	0.0196 ± 0.0004	5.78	1.34
Ni_3Al	Matrix	0.527 ± 0.001	0.0189 ± 0.0003	6.77	2.06
Ni_3Al–Fe	Matrix	0.528 ± 0.002	0.0180 ± 0.0004	6.49	1.80
Fe–Ni–Al (as quenched)	Matrix	0.528 ± 0.002	0.0139 ± 0.0003	6.20	1.60
Fe–Ni–Al (aged 1 h)	Matrix and nanoparticles	0.537 ± 0.001	0.0144 ± 0.0003	6.24	1.61
Fe–Ni–Al (aged 3 h)	Nanoparticles	0.536 ± 0.001	0.0153 ± 0.0003	6.42	1.76
Fe–Ni–Al (aged 22 h)	Nanoparticles	0.535 ± 0.001	0.0167 ± 0.0003	6.41	1.75
Fe–Ni–Al (aged 46 h)	Nanoparticles	0.537 ± 0.001	0.0164 ± 0.0003	6.45	1.78
Fe–Ni–Al (electron irradiated at 300 K to $\Phi = 0.7 \times 10^{18}$ cm^{-2})	Matrix and vacancy-type defects	0.584 ± 0.002	0.0100 ± 0.0004	—	—

concentration being 10^{-6} [25]). This supports theoretical predictions for this compound according to which deviations from the stoichiometric compositions on both sides give rise to antisite atoms rather than to structural vacancies [29, 30]. As far as the third reason is concerned, although pure Ni and the Ni_3Al compound have similar lattice parameters and each atom has the same coordination number of 12 atoms as first-nearest neighbours, in Ni_3Al four Al atoms plus eight Ni atoms surround each Ni atom. Therefore, the density of Ni atoms in the compound is smaller than in pure Ni. Thus, one may think that the height of the 3d peak

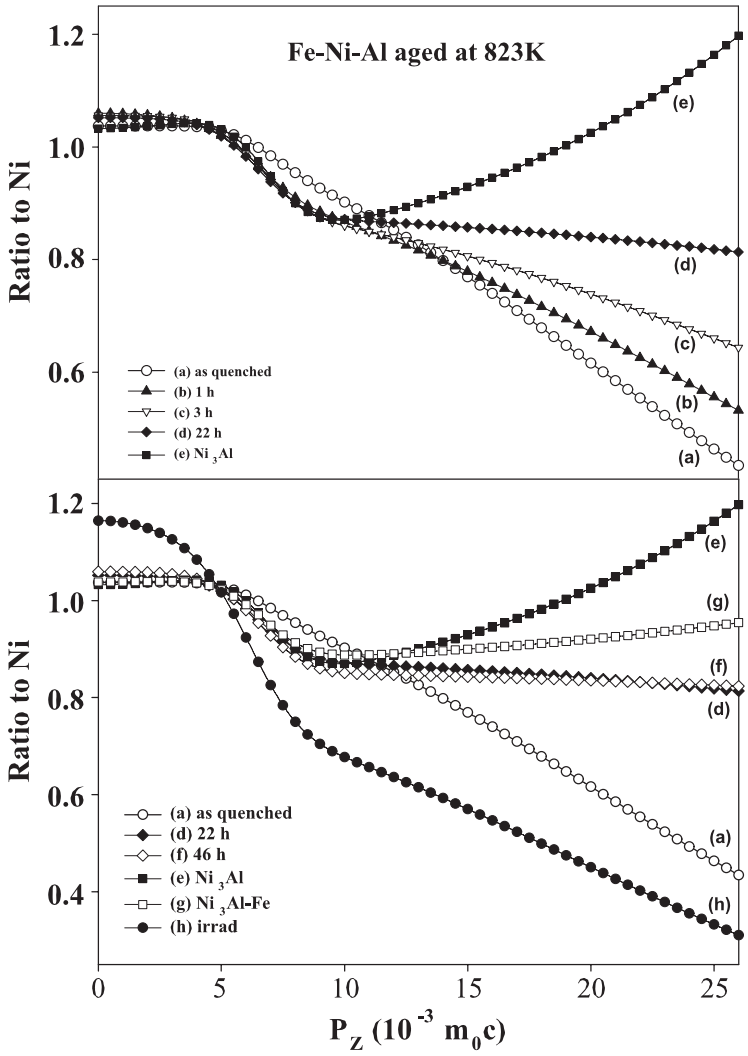

Figure 3. Ratio curves of the ACAR spectra of the Fe–Ni–Al alloys (a) as quenched, after (b) 1 h, (c) 3 h, (d) 22 h, (f) 46 h ageing and (h) as irradiated with a electron fluence of 0.7×10^{18} cm^{-2} with respect to that of Ni. (e, g) Ratio curves for the Ni_3Al and the Ni_3Al–Fe compounds, respectively.

in the ratio curve of the intermetallic was decreased due to both the drop of the Ni density and the formation of a covalent (or iono-covalent [31]) chemical bond.

Information about valence (nearly free) electrons can be obtained from analysis of the parabolic component of the ACAR spectrum. Table 1 gives the NFE number N_p per atom for nickel, bulk intermetallics and nanoparticles calculated using the expression (2). From this table 1 it is seen that the valence electron density in Ni_3Al increased considerably as compared with its counterpart in Ni, i.e. $N_p(Ni_3Al) - N_p(Ni) \approx 0.72$ electrons per atom. Therefore, the parameter N_p can be used for identification of positron states in intermetallic nanoparticles.

Figure 3 presents ratio curves of ACAR spectra of the quenched Fe–Ni–Al alloy and the same alloy but aged at 823 K for 1–46 h, with respect to Ni. Nickel was used as the reference because, as was shown above, positrons annihilated predominantly in the Ni sublattice in

the intermetallic. Figure 3 also gives curves for Fe–Ni–Al, which was exposed to electrons with a fluence of $\sim 0.7 \times 10^{18}$ cm^{-2} at $\sim$300 K and curves for Ni_3Al and Ni_3Al–Fe (bulk) intermetallics. Specific features of positron annihilation in the quenched Fe–Ni–Al alloy have been discussed in the foregoing.

Results obtained for the aged alloy presented a special interest. As the ageing time increased, the probability of annihilation of positrons with electrons of the ion core (at $p_z > 10 \times 10^{-3}\ m_0c$) was enhanced. The shape of the ratio curves approached the shape of the curves obtained for bulk intermetallics. This was a clear indication that positrons in the aged alloy annihilated mainly with nickel electrons.

The TEM examination of the alloy, which was aged for 46 h, revealed the presence of the ordered γ'-phase whose lattice was isomorphous to the lattice of the solid solution. The dimensions and the density of spherical precipitates were determined from dark-field images recorded in superstructural reflections. The particles were $\sim$2.5 nm in size and their density was 3×10^{17} cm^{-3}. At earlier stages of ageing, the dimensions and the density of the particles could not be measured by TEM. Estimates from LSW theory [11] showed that intermetallic particles would be nanosized or subnanosized ($\sim$1 nm) with a density of about 10^{18} cm^{-3} at early stages of ageing (1–3 h). This is a typical density of positron trapping centres, e.g., vacancy-type defects [21], when all positrons annihilate in these centres.

One may state therefore that a quantum-dot-like positron state was realized in intermetallic nanoparticles, similarly to the case for Cu precipitates in an aged Fe–Cu alloy [4]; i.e. the positron density was mainly localized on nanoparticles, which were free of defects. This positron state in the ultrafine particle could be explained in terms of the difference in positron affinity between the precipitates and the matrix [8]. Unfortunately, calculated affinities of positrons A_+ [7] in the Ni_3Al-type intermetallic are not available in the literature and, therefore, it was impossible to estimate the critical radius [6, 7] of particles for formation of the bound state of a positron.

If positrons are trapped at possible open-volume defects such as vacancies or interfaces at the precipitates, the ratio curve will have an enhanced momentum density at the low momentum region due to the annihilations with the electrons within these defects [21]. Indeed, irradiation of the quenched Fe–Ni–Al alloy sharply increased the probability of annihilation with NFEs and, correspondingly, decreased the probability of annihilation with core electrons (see curve h in figure 3). It is seen from table 1 that the S-parameter increased considerably and the W-parameter decreased in the irradiated alloy. Such a situation is typical for positrons being trapped at open-volume defects [16, 21].

When positrons were trapped in nanoparticles, the S-parameter increased insignificantly as compared with the S-parameter of the quenched alloy and the bulk Ni_3Al intermetallic. The W-parameter increased too (see table 1). The simultaneous growth of the S- and W-parameters was due, in our opinion, to specific features of the electronic structure of nanoparticles. Nanoparticles can be viewed as quantum dots. It is known (see [32] and references therein) that electronic properties of quantum dots are considerably modified as compared to the bulk state.

It is seen in figure 3 that the ratio curves of the alloys which were aged for 22 and 46 h coincide. On the other hand, at momenta $p_z > 15 \times 10^{-3}\ m_0c$ these curves (d and f) are far from the curve (namely e) obtained for bulk Ni_3Al. The curves for nanoparticles and bulk Ni_3Al could be different for two reasons: (1) some positrons annihilated in the alloy matrix; (2) the structure and the composition of nanoparticles differed from those of bulk Ni_3Al. According to the estimates, the first reason is less probable. Since the effect of nanoparticles on the ACAR spectra is observed at room temperature, we suppose that particles represent a deep potential well for positrons [6] and the possibility of detrapping can be neglected. In this case,

the diffusion-limited trapping model [12] can be used for calculating the fraction of positrons annihilating in nanoparticles. Assuming spherically shaped nanoparticles, this fraction f_n is given by [6]

$$f_n = k/(k + \lambda_{Fe-Ni-Al}) = 4\pi r_n C_n D_+/(4\pi r_n C_n D_+ + \lambda_{Fe-Ni-Al}) \quad (3)$$

where k is the positron trapping rate with respect to the nanoparticles, $\lambda_{Fe-Ni-Al}$ is the annihilation rate in the quenched Fe–Ni–Al alloy, r_n is the nanoparticle radius, C_n is the density of nanoparticles and D_+ is the diffusion coefficient of positrons.

The annihilation rate in Fe–Ni–Al was determined according to a linear interpolation of the τ_f^{-1} values of the constituent pure metals Fe, Ni and Al [24]. It was equal to 9.6×10^9 s^{-1}. The value for the diffusion coefficient for positrons was taken as equal to 0.7 cm^2 s^{-1} for pure Ni [33], as a typical one for fcc materials. The radius of nanoparticles in the alloy aged for 46 h was 1.3 nm and their density was 3×10^{17} cm^{-3} according to the TEM examination. At earlier stages of ageing the radius and the density of the particles were calculated using the LSW theory [11]. These values were 1 nm and 6.3×10^{17} cm^{-3} in the alloy aged for 22 h. Using the numerical values given above, the fraction of annihilations in nanoparticles, f_n, can be calculated. This yields fractions of 97.2% and 98.3% for 46 and 22 h ageing respectively. Thus, most positrons annihilated in nanoparticles of the alloys aged for 22 and 46 h.

As far as the second reason is concerned, the ratio curves of nanoparticles approached the curve g for the Ni_3Al–Fe compound with 8 at.% Fe rather than the curve e for Ni_3Al with a small nonstoichiometry in the direction of excess nickel (see section 2). According to modern representations (see [9] and references therein), Fe atoms can occupy both Ni and Al sites in Ni_3Al. Since the positron density was concentrated predominantly in the Ni sublattice, the presence of Fe atoms in this sublattice would influence primarily annihilation characteristics. Specifically, the probability of annihilation of positrons with Fe 3d electrons was smaller than that of ones with Ni 3d electrons (see figure 1). Correspondingly, at $p_z > 15 \times 10^{-3}\ m_0 c$, curve g had a smaller intensity than curve e.

Thus, it may be concluded that nanoparticles represented an ordered Ni_3Al phase with addition of Fe atoms. According to the phase diagram of the Fe–Ni–Al system [34], the Ni_3Al intermetallic could contain up to 15 at.% Fe in the solid solution at the ageing temperature of 823 K. A lower intensity of the curves d, f for nanoparticles at momenta $p_z > 15 \times 10^{-3}\ m_0 c$ as compared with intensity of curve g was explained by a larger concentration of Fe in nanoparticles than in the Ni_3Al–Fe compound.

The presence of Fe in the ordered Ni_3Al phase led to a decrease in the number of NFEs N_p (see table 1); i.e. the valence electron density in the Ni_3Al decreased if iron atoms were added. It is seen from table 1 that N_p in nanoparticles was close to N_p in Ni_3Al–Fe.

The structure of subnanosized precipitates was still open after 1 h ageing. Curve b in figure 3 shows that positrons annihilated with both Ni and Fe electrons. This observation confirms the partial trapping of positrons in nanoparticles. However, another interpretation is possible. Positrons were trapped fully, but an intermetallic particle had a high content of Fe atoms at this early stage. It is known [35] that the composition of the γ'-phase in Ni-rich alloys evolves drastically during ageing.

In this study the fcc Fe–Ni–Al alloy served as a model alloy of fast breeder reactor stainless steels. It is well known that intermetallic precipitates play a significant role in retardation of void swelling [36]. However, the mechanism is poorly understood in detail. It was found that the quantum-dot-like positron state could reveal the structure of ultrafine intermetallic precipitates in various Fe–Ni–Al (Ti, Si) model alloys, especially its evolution under irradiation. Detailed results will be reported elsewhere.

4. Conclusion

It was shown that the positron annihilation provides us with a unique method for probing electronic and structural properties of the nanocrystals embedded in materials. It was found that nanoparticles in the matrix of the Fe–Ni–Al system had the structure of Ni_3Al with the addition of Fe atoms. Nanoparticles were three-dimensional and free of defects.

Acknowledgments

This work was performed with financial support from the Russian Foundation for Basic Research (project No 04-02-16053) and the Programme of Support for Leading Scientific Schools (project No NSh-639.2003.2).

References

[1] Eldrup M and Singh B N 1997 *J. Nucl. Mater.* **251** 132–8
[2] Arbuzov V L, Danilov S E, Druzhkov A P and Klotsman S M 1993 *Fiz. Met. Metalloved.* **75** 91–5
Arbuzov V L, Danilov S E, Druzhkov A P and Klotsman S M 1993 *Sov. Phys.—Met. Metallogr.* **75** 286–9 (Engl. Transl.)
[3] Druzhkov A P, Arbuzov V L and Danilov S E 1997 *Fiz. Met. Metalloved.* **83** 118–24
Druzhkov A P, Arbuzov V L and Danilov S E 1997 *Sov. Phys.—Met. Metallogr.* **83** 78–82 (Engl. Transl.)
[4] Nagai Y, Hasegawa M, Tang Z, Hempel A, Yubuta K, Shimamura T, Kawazoe Y, Kawai A and Kano F 2000 *Phys. Rev.* B **61** 6574–8
[5] Nagai Y, Chiba T, Tang Z, Akahane T, Kanai T, Hasegawa M, Takenaka M and Kuramoto E 2001 *Phys. Rev. Lett.* **87** 176402
[6] van Huis M A, van Veen A, Schut H, Falub S V, Eijt S W H, Mijnarends P E and Kuriplach J 2002 *Phys. Rev.* B **65** 085416
[7] Puska M J, Lanki P and Nieminen R M 1989 *J. Phys.: Condens. Matter* **1** 6081–93
[8] Brauer G, Puska M J, Sob M and Korhonen T 1995 *Nucl. Eng. Des.* **158** 149
[9] Lawniczac-Jablonska K, Wojnecki R and Kachniarz J 2000 *J. Phys.: Condens. Matter* **12** 2333–50
[10] Petkov M P, Somoza A, Santos G and Lynn K G 2001 *Mater. Sci. Forum* **363–365** 189–91
[11] Wendt H and Haasen P 1983 *Acta Metall.* **31** 1649–59
[12] Dupasquier A and Mills A P Jr (ed) 1995 *Positron Spectroscopy of Solids* (Amsterdam: Institute of Physics Publishing)
[13] Berko S 1983 *Positron Solid State Physics* ed W Brandt and A Dupasquier (Amsterdam: North-Holland)
[14] Alatalo M, Kauppinen H, Saarinen K, Puska M J, Makinen J, Hautojarvi P and Nieminen R M 1995 *Phys. Rev.* B **51** 4176–85
[15] Asoka-Kumar P, Alatalo M, Ghosh V J, Kruseman A C, Nielsen B and Lynn K G 1996 *Phys. Rev. Lett.* **77** 2097–100
[16] Arbuzov V L, Danilov S E and Druzhkov A P 1997 *Phys. Status Solidi* a **162** 567–73
[17] Druzhkov A P, Gizhevskii B A, Arbuzov V L, Kozlov E A, Shalnov K V, Naumov S V and Perminov D A 2002 *J. Phys.: Condens. Matter* **14** 7981–90
[18] Akshentsev Yu N, Stepenova N N, Sazonova V A and Rodionov D P 1997 *Fiz. Met. Metalloved.* **84** 130–7
Akshentsev Yu N, Stepenova N N, Sazonova V A and Rodionov D P 1997 *Sov. Phys.—Met. Metallogr.* **84** 293–8 (Engl. Transl.)
[19] Rempel A A, Druzhkov A P and Gusev A I 1989 *Fiz. Met. Metalloved.* **68** 271–9
Rempel A A, Druzhkov A P and Gusev A I 1989 *Sov. Phys.—Met. Metallogr.* **68** 59–68 (Engl. Transl.)
[20] Debowska E and Rudzinska-Girulska J 1988 *Phys. Status Solidi* b **148** 227–31
[21] Siegel R W 1980 *Annu. Rev. Mater. Sci.* **10** 393–425
[22] Ghosh V J, Alatalo M, Asoka-Kumar P, Nielsen B, Lynn K G, Kruseman A C and Mijnarends 2000 *Phys. Rev.* B **61** 10092–9
[23] Schaefer H-E, Wurschum R and Bub J 1992 *Mater. Sci. Forum* **105–110** 439–50
[24] Wurschum R, Badura-Gergen K, Kummerle E A, Grupp C and Schaefer H-E 1996 *Phys. Rev.* B **54** 849–56
[25] Badura-Gergen K and Schaefer H-E 1997 *Phys. Rev.* B **56** 3032–7
[26] Petegem S V, Zhurkin E E, Mondelaers W, Dauwe C and Segers D 2004 *J. Phys.: Condens. Matter* **16** 591–603

[27] Nautiyal T and Auluck S 1992 *Phys. Rev.* B **45** 13930–7
[28] Xu J H, Min B I, Freeman A J and Oguchi T 1990 *Phys. Rev.* B **41** 5010–6
[29] Badura K and Schaefer H-E 1993 *Z. Metallk.* **84** 405
[30] Fu C L and Painter G S 1997 *Acta Metall. Mater.* **45** 481
[31] Ito O and Tamaki H 1995 *Acta Metall. Mater.* **43** 2731–5
[32] Saniz R, Barbiellini B and Denison A 2002 *Phys. Rev.* B **65** 245310
[33] Schultz P J and Lynn K G 1988 *Rev. Mod. Phys.* **60** 701–79
[34] Masahashi N, Kawazoe H, Takasugi T and Izumi O 1987 *Z. Metallk.* **78** 788–94
[35] Duval S, Chambreland S, Caron P and Blavette D 1994 *Acta Mater.* **42** 185–94
[36] Sagaradse V V, Nalesnik V M, Lapin S S and Aljabiev V M 1993 *J. Nucl. Mater.* **202** 137–44